Astronomy & Astrophysics manuscript no. May 9, 2003
(DOI: will be inserted by hand later)

Spectroscopic homogeneity of Type Ia SNe measured through equivalent widths

G. Folatelli, G. Garavini, A. Goobar, S. Nobili,...

Department of Physics, Stockholm University,
SCFAB, SE–106 91 Stockholm, Sweden

Received ...; accepted ...

Abstract. We present a study of spectral homogeneity performed with equivalent width (EW) measurements on a sample of over 150 spectra belonging to 21 low-z SNe Ia which were followed roughly from 15 days before maximum brightness to 60 days after. Eight spectral features at optical wavelengths are defined and their EW are followed throught the first months after the explosion. We find that some of those features show a remarkably homogeneous evolutionary behavior, with systematic differences correlated with lightcurve shape. Features due to Si II show the clearest quantitative distinction between spectroscopically normal and peculiar SNe Ia. A sequence of decreasing EW's from under-luminous, through normal to 1991T/1999aa-like SNe is found. New spectral parameters are introduced and their correlation with $\Delta m_{15}(B)$ are presented.

Key words.

1. Introduction

Type Ia supernovæ (SNe Ia) have been used as standard candles for distance measuremets and thus to probe the expansion history of the Universe. Although the results from two independent teams favor a Λ-*dominated* Universe (Perlmutter et al., 1999; Riess et al., 1998; Sullivan et al., 2003; Tonry et al., 2003; Knop et al., 2003), the physical nature of SNe Ia as such is not well understood. The nature of the secondary component in the binary system as well as the explosion and radiative transport mechanisms leading to a supernova event are still open questions (see a review in Hillebrandt & Niemeyer (2000)). Furthermore, systematic effects of evolutionary or environmental origin have been proposed as alternatives to the cosmological explanations to the dimness of the high-z SNe Ia. Besides lightcurve shapes, spectroscopic studies provide the most effective means for testing the standard candle hypothesis in detail.

Classification and *qualitative* analysis of Type Ia spectra are a first and important step in the progress toward an understanding of SN Ia (Filippenko, 1997; Gómez et al, 1996; Gómez & López, 1998). Nevertheless, a deeper and more comprehensive knowledge must come from *quantitative* studies. A few attempts have been made in the search for correlations between spectral characteristics – line strengths, blueshifts, etc.– and lightcurve properties, attaining in some cases partial theoretical explanations as-

Send offprint requests to: Gastón Folatelli; gaston@physto.se

sociated with physical properties of the SNe (Nugent et al., 1995; Hatano et al., 2000). **Mention work on individual SNe and diff. kinds of models?**. The nature of this analysis is at this stage purely empirical. It is motivated in the fact that, when compared with spectroscopically normal SNe Ia, under-luminous SNe generally show stronger absorptions at photospheric phases while other peculiar objects which can be classified as 1991T- and 1999aa-like show weaker absorptions. Based on a large spectroscopic sample, which includes several of the peculiar SNe, the goals of this work are threefold: (a) Quantify the spectral homogeneity of SNe Ia. (b) Provide empirically derived time evolution of spectroscopic features to facilitate the work of SN modelers. (c) Look for secondary spectral calibrators to sharpen the standard candle nature of SNe Ia. This work is also thought to set the bases for a novel manner to compare spectral characteristics of nearby and high-redshift SNe. Rigurosity in the treatment of uncertainties is possible thanks to the spectroscopy with associated error estimates presented in Folatelli et al. (2003). Other spectroscopic measurements (line intensity ratios, line widths, blueshifts of the minima, etc.) will complement this analysis in forthcoming work. A more thorough physical interpretation of the data should come as SN models improve.

Section 2 briefly describes the two sets of spectroscopic data used in this work. Section 3 introduces the definitions on which the measurements in this work are based and the way systematic errors were controlled and final uncertainties estimated. Section 4 presents the analysis of the those results. Finally, Sec. 5 summarizes the achievements of this work and comments on its future prospects. **(confirm section descriptions)**

2. Data description

The results shown in this paper come from two sets of spectroscopic data: Set A - 77 spectra from 13 SNe Ia discovered and followed by the Supernova Cosmology Project (SCP) in collaboration with members of the EROS (Hardin et al., 2000), the QUEST (Schaefer et al., 1999), and the Nearby Galaxies SN Search (Gal-Yam et al., 1999) teams. More details about these data can be found in Table 1; Set B - 89 published spectra from 8 well-observed, nearby objects. See Table 2 for details on these data.

Data from Set A were reduced and processed according to the method described in Folatelli et al. (2003). They consist of flux-calibrated spectra which were additionally corrected for atmospheric and galactic extinction (Cardelli et al., 1989; Schlegel et al., 1998). They were compared to photometry and corrected when discrepancies were greater than the estimated calibration uncertainties (typically in the range of 5 to 10% of the total flux). All these spectra include estimated statistical uncertainties for each wavelength bin. A subset of these spectra showed some degree of host galaxy light contamination. This contribution was estimated and subtracted in cases where it exceeded 10% of the total flux.

The spectra from Set B were taken from **(Add a list of sources)**. These spectra were originally all flux-calibrated. Those calibrations were tested and corrected when needed by use of available photometry. Given the absence of uncertainties on these spectra, mean Poisson errors were estimated from point-to-point dispersion.

3. Measurement description

3.1. Feature definitions

Based on the typical distribution of absorption features from near-maximum SN Ia spectra, eight measuring regions bounded by spectral flux maxima have been defined.

Table 1. SNe from Set A.

SN	z	Galaxy	Gal. type	Epochs
1999aa	0.0144	NGC 2595	SAB(rs)c	-11,-3,-1,5,6,14,19,25,28,33,40,47,51,58
1999ac	0.0095	NGC 6063	Scd	-15,-9,0,2,8,11,16,24,28,31,33,39,42
1999ao	0.054	Anon.	S	5,7,10,13,18,34,40
1999au	0.124	Anon.	S	12,17
1999av	0.05	Anon.	E/S0	2,5,9,31
1999aw	0.04	Anon.	(?)	3,5,9,12,16,24,31,38
1999be	0.019	Anon.	(?)	14,19,26,33,37,44
1999bk	0.096	Anon.	E/S0	4,7,9
1999bm	0.143	Anon.	S	3,6,21
1999bn	0.129	Anon.	S	2,14,22
1999bp	0.077	Anon.	S	-2,0,1,6,17,23
1999bq	0.149	Anon.	E/S0	3,18
1999by	0.0021	NGC 2841	SA(r)b	1,6,16,27,34

Table 2. SNe from Set B.

SN	z	Galaxy	Gal. type	Epochs	Sources[a]
1981B	0.006031	NGC 4536	SAB(rs)bc	0,17,26,29,35	(3)
1986G	0.001825	NGC 5128	SO pec	-7,-5,-1,0,3,21,28,41,44,55	(1) (3)
1989B	0.002425	NGC 3627	SAB(s)b	-7,-5,-3,-2,-1,3,5,8,9,11,13,16,18,19	(1) (3)
1990N	0.003369	NGC 4639	SAB(rs)bc	-14,-7,7,14,17,38	(1), (3)
1991bg	0.003536	NGC 4374	E1	-2,0,13,16,23,24,30,31,44,52	(1)
1991T	0.005791	NGC 4527	SAB(s)bc	-11,-9,-8,-7,-6,-5,-3,0,10,15,23,24,42,45	(1) (3)
1992A	0.006261	NGC 1380	SA0	-5,-1,3,5,7,9,11,16,17,24,28,37,46	(3)
1994D	0.00149	NGC 4526	SAB(s)	-10,-9,-8,-7,-5,-3,2,4,6,8,11,13,14,16,18,20,25	(1)

[a] (1) Asiago SN Catalog; (2) G. Gómez & R. López (AJ, 115, 1998); (3).

Figure 1 shows these regions as they are defined at different epochs. The label names in some cases correspond to the actual identification of the elements producing the features, although in general they are thought as purely mnemonic names. This becomes evident as we advance to times later than a week after maximum light and line identifications change, or lines that once were separated become blended together and are later on considered as part of the same feature. Around a month after maximum light emission lines start to dominate; nevertheless, feature definitions are kept as "absorptions" between emission maxima. As a consequence of spectral evolution, wavelength limits for each feature may vary as a function of time. Differences from object to object are also expected, especially in the case of peculiar SNe. Additionally, some of the weaker features may not be present for some objects or might disappear at some epochs. That is the case of features "Si II 4000" and "Si II 5800". They are ab-

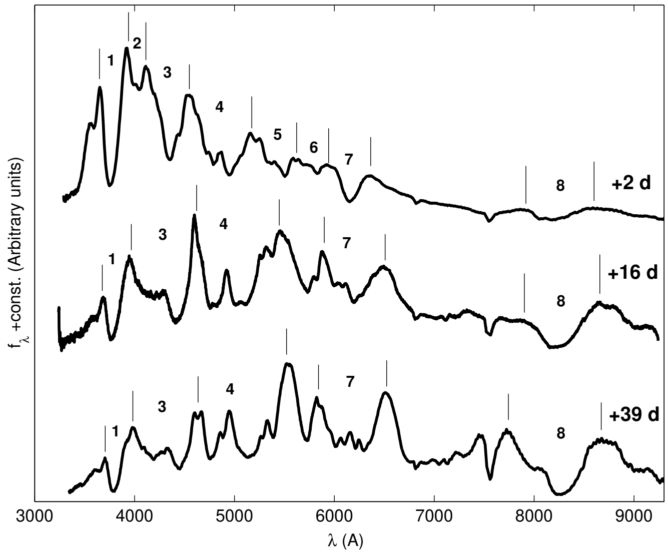

Fig. 1. SNe Ia spectral evolution and feature definitions for three epochs: 2, 16 and 39 days after maximum light. Numerical labels correspond to feature names: **1**- "Ca II H&K"; **2**- "Si II 4000"; **3**- "Mg II 4300"; **4**- "Fe II 4800"; **5**- "S II W"; **6**- "Si II 5800"; **7**- "Si II 6150"; and **8**- "Ca II IR". Vertical lines show the positions where the pseudo-continuum is taken. It can be seen how features defined as such evolve in time and how some weaker features are not considered at later epochs. It is clear that, as the SNe leave the photospheric phase, pseudo-continuum points correspond to emission peaks.

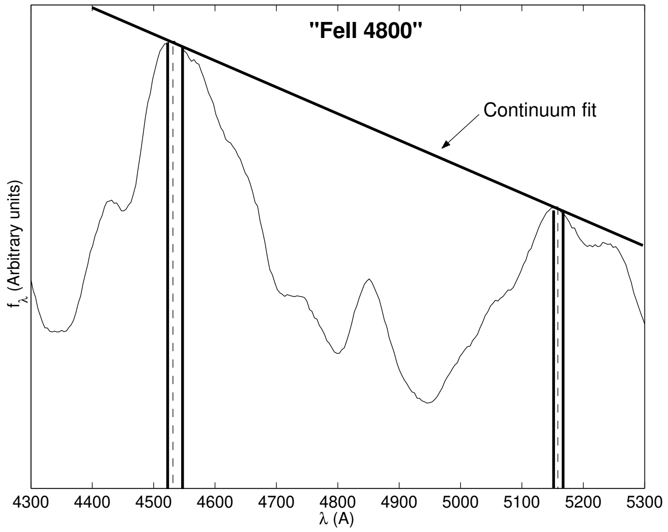

Fig. 2. Example of a local continuum fit around a feature. Solid vertical lines show the regions where the fit is performed. Dashed vertical lines mark the measurement limits.

sent or very faint in the case of 1991T/1999aa-like SNe Ia (where we include SN 1999aw (Strolger et al., 2002) and SN 1999bp). In all cases they eventually become blended with neighboring features. "S II W" is only defined while it keeps its characteristic "W" shape.

3.2. Equivalent widths

In order to measure equivalent widths (EW), the continuum flux level bracketing each feature must be determined. However, this not always possible in SNe Ia due to the nature of their broad line-dominated spectra. When the determination of the actual continuum level could not be achieved, the two points of maximum flux that define the feature limits were taken as pseudo-continuum points. The continuum was then traced by least-squares fit of a straight line through points selected in two regions, each one around a maximum (see Fig. 2). **Maybe make an inlay of Fig. 2 in Fig. 1**.

Once the continuum is traced, the EW is computed for each feature within its wavelength limits. The spectrum is normalized by the continuum and the resulting area of the absorption feature is measured (in units of Å). In this case, the calculation was approximated by a simple rectangular integration method:

$$\mathrm{EW} = \sum_{i=2}^{N} \left(1 - \frac{f_\lambda(\lambda_i)}{f_c(\lambda_i)}\right) \Delta\lambda_i, \tag{1}$$

where λ_i $(i = 2, \ldots, N)$ are the binned wavelength values within the feature limits, with intervals $\Delta\lambda_i = \lambda_i - \lambda_{i-1}$; $f_\lambda(\lambda_i)$ is the measured flux in each bin i; $f_c(\lambda_i)$ is the fitted continuum flux evaluated at the same points.

A 1σ statistical uncertainty was computed by error propagation from the estimated errors in the spectral flux and in the fitted continuum:

$$\sigma_{\mathrm{EW}} = \left[\sum_{i=2}^{N} \left(\frac{\sigma^2_{f_i}(\lambda_i)}{f_c^2(\lambda_i)} + \frac{f_\lambda^2(\lambda_i)}{f_c^4(\lambda_i)}\sigma^2_{c_i}(\lambda_i)\right)(\Delta\lambda_i)^2\right]^{1/2}. \tag{2}$$

Here, σ_{f_i} are the estimated measurement uncertainties on spectral flux and σ_{c_i} are the uncertainties in the fitted continuum flux. In the calculation of $\sigma_{\rm EW}$, it was assumed that values in different wavelength bins are independent from each other and numerical uncertainties arising from the integration method itself were neglected.

Additionally, systematic errors in the determination of the continuum were accounted for by performing the fits on sliding windows and computing the weighted root-mean square deviation (rms) of the encountered EW's. This source of error was added to the one given in Eqn. 2.

It should be enphasized that these EW's were measured based on the empirical determination of a pseudo-continuum level along each feature. The nature of SN spectra makes the interpretation of these measurements different from those performed on single, narrow lines of stars. This does not prevent us from building well-defined quantities and thus a consistent set of measurements, based on the systematic manner in which that level is determined.

By definition, EW is distance-independent and thus provides the ideal tools to compare spectra from different objects. Section 4 is dedicated to this analysis.

3.3. Checks for systematics

It is known that EW's can be affected by poor resolution or signal-to-noise on the spectra (Gray, 1992). These effects were tested by artificially treating the spectra. Boxcar smoothing was used to worsen the resolution of the best-sampled spectra. Because of the nature of the broad SN features, even the worst resolution available ($\sim$10 Å/pixel) proved not to produce any change on the measured EW. Signal-to-noise ratios ranged roughly from around 5 to several hundreds. When Gaussian noise was added to the best-quality spectra in order to reproduce that quality range, no bias was detected on the resulting EW values. Finally, the effect of reddening was also tested by artificially adding it up to a value of $E(B-V) = 0.32$ (corresponding to $A_V = 1$ mag, with $R_V = 3.1$) following the law given in Cardelli et al. (1989). This produced no change in the final values for EW. The nature of the EW measurements, given by the point-to-point ratio of observed to continuum fluxes, makes them unsusceptible to reddening.

4. Spectral evolution

A first use of EW's is the study of their change in time as a way to characterize spectral evolution. Though empirically defined, consistency in the measurements allow for a comparative analysis which can shed light on supernova models and may yield new spectral parameters for an improvement in their use as standard candles. As the SN evolves from its first hot stages of free expansion, through maximum light, and finally into the nebular phase, both continuum and line properties vary. Temperature variations as well as the receding of the photosphere in the ejecta (Hillebrandt & Niemeyer, 2000) translate into changes in EW values.

The following analysis is divided by features. The first three sections are dedicated to features which show the greatest homogeneity, even including peculiar SNe: "Fe II 4800", "Ca II IR", and "Mg II 4300". "Fe II 4800" and "Mg II 4300" fall in a region of the spectrum where several ions of intermediate-mass and iron-peak elements contribute to form fairly complex profiles (Branch et al., 1983). "Ca II IR" on the contrary is supposed to be due to the Ca II infrared triplet at all epochs, with little contamination from other ions. Subsequent sections involve features with more heterogeneous behavior, i.e. the three "Si II" features, "Ca II H&K" and "S II W". These features are believed to be formed by intermediate-mass elements around maximum light and eventually become contaminated by iron-peak element lines (Branch et al., 1983; Filippenko, 1997).

It should be mentioned that the epochs used in this analysis are based on photometry data. In the case of SCP data, preliminary light-curves were used for determining the date of maximum B brightness and epochs were corroborated to within a few days by spectral shape comparison with precisely dated SNe. Epochs were considered for simplicity and evenness of the data sample as an integer number of days.

4.1. "Fe II 4800"

This feature shows a very smooth evolution for all SNe (see Fig. 3). EW's from different objects show almost parallel evolutionary traces as they increase from around 100Å before maximum light to 350Å 25 days after, with some hint for a decline from then on. At epochs later than 15 days, this feature has become blended together with lines lying to the red of it (see Fig. 1). The moment when this blending takes place depends on the object: it is later for peculiar SNe like SN 1999aa and SN 1999aw and earlier for the under-luminous SN 1999by. A mean evolutionary pattern can be represented by a cubic spline function. This function was built by dividing the data into 5 bins, calculating a weighted average in each bin and finally tracing the spline function through those points. Individual objects evolve approximately parallel to the mean curve. Under-luminous SNe lie above the curve and 1991T/1999aa-like SNe lie below it. A clear trend can be put in terms of increasing EW with increasing $\Delta m_{15}(B)$: SNe 1999aw/1999bp, SNe 1991T/1999aa, normal SNe, SNe 1986G/1991bg/1999by. This is seen in Fig. 4 where for each SN $\Delta m_{15}(B)$ is plotted against the weighted mean of the deviations from the model, $\langle\Delta \mathrm{EW}\rangle_{\mathrm{Fe\,II}\,4800}$, for EW points between days 0 and 30. $\Delta m_{15}(B)$ values were calculated from published and preliminary lightcurves using

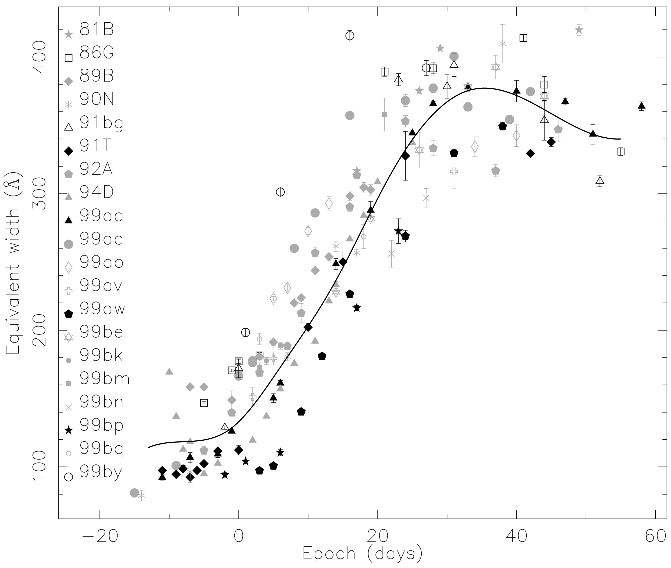

Fig. 3. Measured EW values corresponding to "Fe II 4800". Error-bars are given by Eqn. 2 plus systematics arising in the continuum fit. The solid line represents a cubic spline function used to model the evolution of "Fe II 4800" EW. Open, black symbols are used for under-luminous SNe; gray symbols for normal SNe; filled, black symbols for 1991T/1999aa-like SNe.

a consistent fitting technique. A correlation between these two quantities was found and represented by a linear function fitted by least-squares:

$$\Delta m_{15}(B) = 1.04(\pm0.03) + 0.0095(\pm0.0008) \times \langle\Delta \mathrm{EW}\rangle_{\mathrm{Fe\,II}\,4800}, \quad (3)$$

where $\langle\Delta \mathrm{EW}\rangle_{\mathrm{Fe\,II}\,4800}$ is given in Å.

An intrinsic dispersion for all the SNe was computed as the weighted standard deviation around the average model in time bins of 5 days. Results are shown in Table 3. The mean evolutionary curve and the estimated dispersion around it can be used in order to characterize a certain SN with respect to the rest at any epoch. It can be seen from Table 3 that a dispersion of around 30Å is found at all epochs and, as EW's increase, the relative dispersion (given in column 5) is significantly smaller after day 15, below 10%.

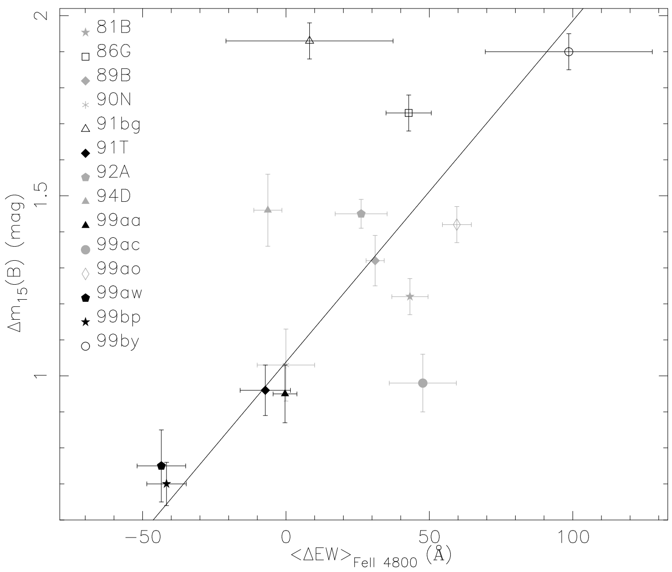

Fig. 4. Weighted mean EW deviations, $\langle\Delta\text{EW}\rangle_{\text{Fe II }4800}$, from the "Fe II 4800" model between days 0 and 30 and their correlation to the photometric parameter $\Delta m_{15}(B)$ for different SNe.

4.2. "Ca II IR"

This feature, usually assigned to a Ca II triplet with very little contamination from other elements, shows an evolutionary pattern which is similar to that of "Fe II 4800" (see Fig. 5). Fewer spectra in this sample cover the region spanned by this broad feature (approximately 7800Å to 8600Å), which reduces the statistical significance of these results. Fringing residuals and sensitivity cut-off from some detectors may introduce higher noise and systematic uncertainties by affecting the position and level of the continuum. These effects have been controlled and problematic data excluded from the analysis.

Similarly to "Fe II 4800", EW's start growing at maximum light and stabilize after approximately day 25, though the amplitude of the increase is greater in this case. Individual objects evolve in a nearly parallel manner, lying on either side of an average evolutionary curve. Again, a cubic spline function gives the average model shown in Fig. 5. The family of under-luminous SNe (SN 1986G, SN 1991bg and SN 1999by) was excluded from

Table 3. Dispersion of "Fe II 4800".

Epoch bin (1)	N (2)	⟨EW⟩ (3)	Δ_{EW} (4)	$\Delta_{\text{EW}}/\langle\text{EW}\rangle$ (5)
[−12, −8]	8	129. ± 19.	34. ± 8.	0.26
[−7, −3]	14	110. ± 10.	24. ± 4.	0.22
[−2, 2]	16	156. ± 10.	31. ± 3.	0.20
[3, 7]	21	157. ± 15.	30. ± 10.	0.19
[8, 12]	14	198. ± 19.	37. ± 11.	0.19
[13, 17]	17	236. ± 25.	21. ± 21.	0.09
[18, 22]	10	294. ± 12.	14. ± 17.	0.05
[23, 27]	12	341. ± 19.	14. ± 18.	0.04
[28, 32]	10	380. ± 13.	30. ± 5.	0.08
[33, 37]	6	369. ± 14.	20. ± 15.	0.05
[38, 42]	8	363. ± 16.	27. ± 7.	0.07
[43, 47]	6	361. ± 10.	16. ± 2.	0.04

(1): Epoch range in bin. (2): Number of points in bin. (3): Weighted average of EW's in bin and its 1σ uncertainty. (4): Intrinsic dispersion of EW's in bin from model and its uncertainty. (5): Ratio of the intrinsic dispersion to the mean EW in bin.

the sample used to build the average curve. This time the spline function was determined using 4 points. The same trend of increasing EW with increasing $\Delta m_{15}(B)$ pointed out in the case of "Fe II 4800" is seen here, as shown in Fig. 6 which is analogous to Fig. 4. Again, weighted mean deviations, $\langle\Delta\text{EW}\rangle_{\text{Ca II IR}}$, from the model were computed for each SN separately considering the time range from maximum light to 30 days after. Fewer SNe presented enough data to allow the calculation. However, a least-squares fit of a straight line was done in order to represent a correlation between $\langle\Delta\text{EW}\rangle_{\text{Ca II IR}}$ (expressed in Å) and $\Delta m_{15}(B)$:

$$\Delta m_{15}(B) = 0.97(\pm 0.04) + 0.0061(\pm 0.0007) \times \langle\Delta\text{EW}\rangle_{\text{Ca II IR}}. \quad (4)$$

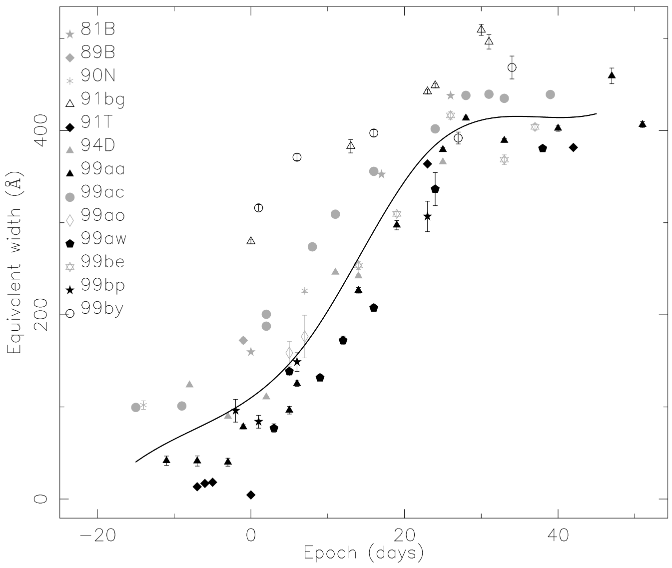

Fig. 5. Measured EW values corresponding to "Ca II IR". Error-bars are given by Eqn. 2 plus systematics arising in the continuum fit. The solid line represents a cubic spline function used to model the mean evolution of "Ca II IR". Under-luminous SNe were excluded when building the model.

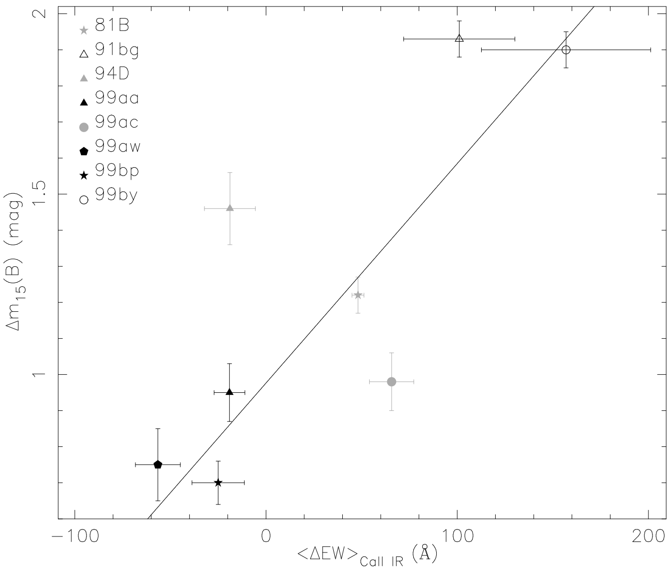

Fig. 6. Weighted mean EW deviations, $\langle\Delta\mathrm{EW}\rangle_{\mathrm{Ca\,II\,IR}}$, from the "Ca II IR" model between days 0 and 30 and their correlation to the photometric parameter $\Delta m_{15}(B)$ for different SNe. A straight-line fitted to the correlation is shown.

Table 4. Dispersion of "Ca II IR" EW's. See column explanations in Table 3. Under-luminous SNe are excluded.

Epoch bin	N	$\langle$EW$\rangle$	Δ_{EW}	$\Delta_{\mathrm{EW}}/\langle\mathrm{EW}\rangle$
(1)	(2)	(3)	(4)	(5)
$[-5, 1]$	8.	84. ± 45.	24. ± 26.	0.29
$[2, 8]$	12.	147. ± 51.	46. ± 22.	0.31
$[9, 15]$	7.	259. ± 24.	56. ± 16.	0.22
$[16, 22]$	5.	339. ± 25.	56. ± 8.	0.17
$[23, 29]$	10.	373. ± 21.	24. ± 4.	0.06
$[30, 36]$	4.	420. ± 21.	24. ± 5.	0.06

Dispersion values around the average curve can be seen in Table 4, where under-luminous SNe are not included. Due to poorer statistics, in this case time coverage is limited to day 35 and coarser bins had to be taken. The same behavior that was seen for "Fe II 4800" is seen here: an overall dispersion of around 30Å and relative dispersions decreasing to below 10% after two weeks from maximum light.

An important characteristic of this feature is that it is believed to be due to the Ca II IR triplet at all epochs (Branch et al., 1983; Filippenko, 1997) (**refs...**). Studies of this feature may thus prove to yield some direct information on the physics of the ejecta.

This feature covers approximately a half of the standard I-band filter range. Therefore, one may expect to find correlations between EW measures and I magnitudes. This point is left for future study.

4.3. "Mg II 4300"

This feature is formed at different epochs by the overlap of lines from various ions. These include Mg II, Co II, Fe II, Fe III, and Si III for spectroscopically normal and 1991T/1999aa-like SNe (**refs...**). In the case of under-luminous SNe, the region is dominated by strong lines due to Ti II (Filippenko et al., 1992; Mazzali et al., 1997). Its EW evolution is not as smooth as in the two previous cases. As can be seen in Fig. 7, a more or less discontinuous evolutionary behavior is found here. This is related to blending with "Si II 4000" in coincidence with absorption deepening which makes EW's suddenly increase from ~ 100Å to ~ 260Å on time scales of less than a week. The moment when this break takes place is highly dependent on the kind of object: under-luminous SNe Ia seem to be on the rise as early as 5 days before maximum (the earliest spectrum we have of SN 1986G), while normal SNe Ia show this behavior around one week after maximum, and 1991T/1999aa-like objects show it later than day 10. This causes remarkable EW differences between under-luminous SNe and the rest at times around maximum light.

The average behavior can be represented by a function:

$$f(\boldsymbol{\theta}, t) = \frac{A}{e^{\frac{t_0 - t}{\tau}} + 1} + B, \qquad (5)$$

whose parameters $\boldsymbol{\theta} = (A, B, t_0, \tau)$ can be fitted from the data. The fit was performed excluding the extreme cases of under-luminous SNe: SN 1986G, SN 1991bg and SN 1999by, and SN 1999aw. Again, nearly parallel evolutionary paths are followed by individual SNe varying systematically among SN families as in the cases of the two previous features. The dispersion of points around the average model is computed for the sample and results are shown in Table 5. Greater dispersion around day 10 reflects differences in the moment when the break occurs.

The same kind of model can be fitted to individual SNe in order to parametrize and compare their behavior. In particular, the parameter t_0, which corresponds to the epoch when the EW is half-way on its rise, clearly correlates with photometric characteristics. t_0 is greater for SNe with slower light-curves. Figure 8 shows $\Delta m_{15}(B)$ plotted against t_0 for different objects together with a straight line fitted by least-squares. In the cases of SN 1991bg and SN 1999by upper limits for t_0 are given as the epochs of their earliest spectra, assuming they followed the same evolution pattern found for other objects. The fit was done excluding the two upper limits and the interesting case of

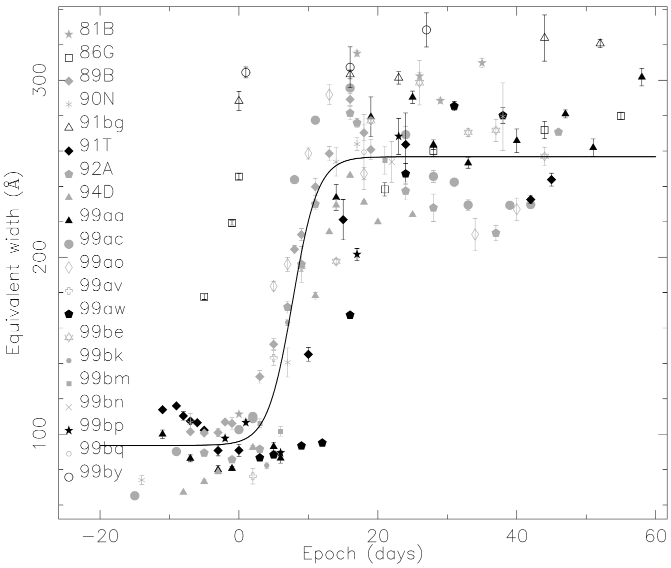

Fig. 7. Measured EW values corresponding to "Mg II 4300". Error-bars are given by Eqn. 2 plus systematics arising in the continuum fit. The solid line represents the modeled mean behavior of normal SNe Ia, fitted using the function of Eqn. 5 and excluding SN 1986G, SN 1991bg, SN 1999by and SN 1999aw.

SN 1999ac, which deviates by more than 5 sigma. This SN presents photometric and spectroscopic peculiarities which make it a unique object: its light-curve shows a slow rise similar to SN 1991T but a fast decline (Phillips et al., 2002) and its spectrum is 1999aa-like (Garavini et al., 2003). The result of the fit is, for t_0 given in days:

$$\Delta m_{15}(B) = 1.869(\pm 0.052) - 0.070(\pm 0.005) \times t_0. \qquad (6)$$

It should be emphasized that this spectral feature lies almost exactly on the wavelength covered by the standard B filter. A correlation between B light-curves and the evolution of "Mg II 4300" might then be expected. An additional point to note is that this feature can be observed with optical detectors up to redshifts of around 1, which may make studies of this spectral region important for future SN-related cosmology experiments.

Table 5. Dispersion of "Mg II 4300" EW's. See column explanations in Table 3. SN 1986G, SN 1991bg, SN 1999by and SN 1999aw are excluded.

Epoch bin	N	⟨EW⟩	$\Delta_{\rm EW}$	$\Delta_{\rm EW}/\langle{\rm EW}\rangle$
(1)	(2)	(3)	(4)	(5)
$[-12,-8]$	6.	106. ± 24.	23. ± 2.	0.22
$[-7,-3]$	13.	98. ± 5.	10. ± 2.	0.10
$[-2,2]$	13.	102. ± 5.	9. ± 2.	0.09
$[3,7]$	15.	112. ± 14.	37. ± 6.	0.33
$[8,12]$	11.	229. ± 16.	46. ± 7.	0.20
$[13,17]$	16.	235. ± 22.	33. ± 8.	0.14
$[18,22]$	10.	236. ± 14.	29. ± 4.	0.12
$[23,27]$	8.	237. ± 38.	34. ± 4.	0.14
$[28,32]$	5.	265. ± 14.	23. ± 5.	0.09
$[33,37]$	7.	263. ± 15.	31. ± 8.	0.12
$[38,42]$	6.	231. ± 4.	26. ± 1.	0.11
$[43,47]$	4.	271. ± 11.	14. ± 3.	0.05

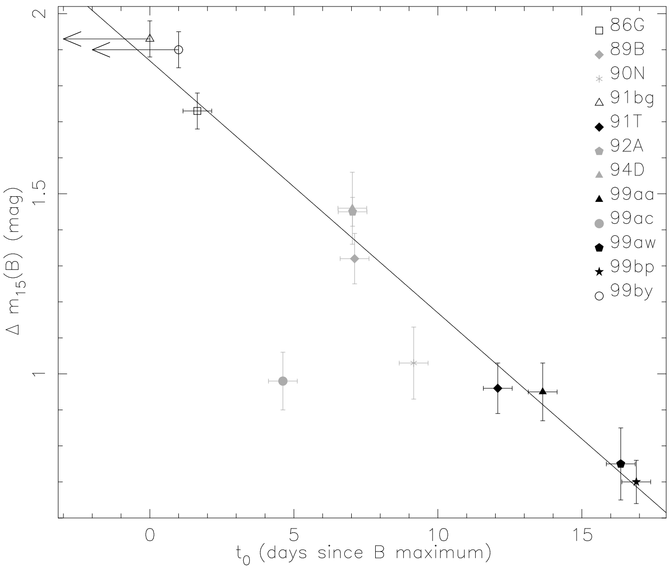

Fig. 8. Straight-line fit to $\Delta m_{15}(B)$ versus t_0 (see text for parameters). Though nominal error-bars in t_0 are below 0.05, a more realistic value of 0.5 was taken, given the dating uncertainties. t_0 values for SN 1991bg and SN 1999by are upper limits taken from the earliest spectrum available and assuming they followed the same behavior as the rest at earlier epochs.

4.4. "Si II*" features*

This section is dedicated to three features which are assigned to Si II in near-maximum spectra and which are peculiar to SNe Ia: "Si II 4000", "Si II 5800" and "Si II 6150" (Branch et al., 1983). Figures 9, 10 and 11 respectively show their EW's. These features are relatively weaker and more subject to contamination than the others treated in this work . "Si II 4000" blends with lines of "Mg II 4300" a few days after maximum and is thereafter considered as part of it. "Si II 4000" is not considered in under-luminous SNe because of the presence of strong Ti II which blends it into a broad "Mg II 4300" feature. In the case of, it "Si II 5800" becomes contaminated by the Na I D line around a week after maximum (Branch et al., 1983) and blends with "S II W". "Si II 6150" remains defined as such for later epochs, though Fe II lines on each side of it appear around 10 days past maximum and the feature becomes broader and structured. The analysis of these features is important as SiII II lines are used to classify SNe Ia as such. The pair "Si II 6150" - "Si II 5800" can be easily identified in optical spectra of low redshift SNe. When going to higher redshift ($z > 0.5$) classification based on optical spectra relies on "Si II 4000". This has to be taken into account when classifying under-luminous SNe Ia at high redshifts (**refs...**).

Dispersion in EW is greater for these features, as they show a clearer distinction among different kinds of SNe Ia. Single objects show increasing EW evolution, as is seen in other features, though in these cases no clear common behavior can be established for the whole set of SNe.

EW measurements of "Si II 4000" between days −10 and 10 for normal and 1991T/1999aa-like SNe show a clear division into two families: (a) A group of SNe with very weak absorptions (EW < 10Å), including the 1991T/1999aa-like objects and SN 1990N. In this group, SN 1999aw is an extreme case. (b) A group of normal

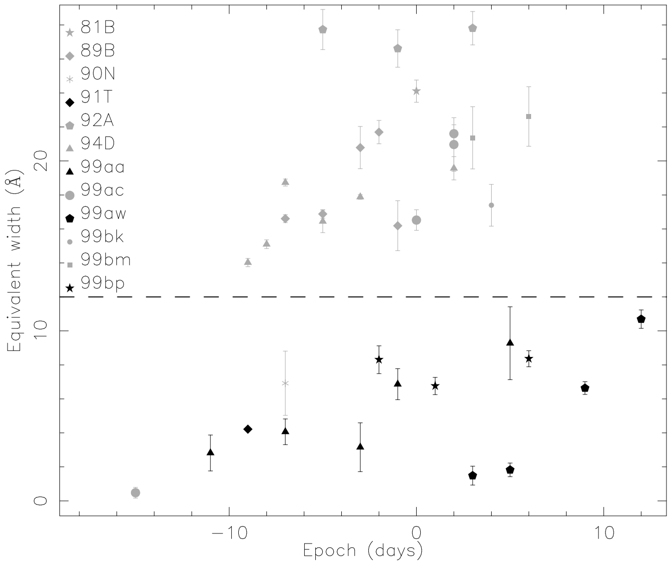

Fig. 9. Measured EW values corresponding to "Si II 4000". Error-bars are given by Eqn. 2 plus systematics arising in the continuum fit. The dashed line divides two families of SNe (see text).

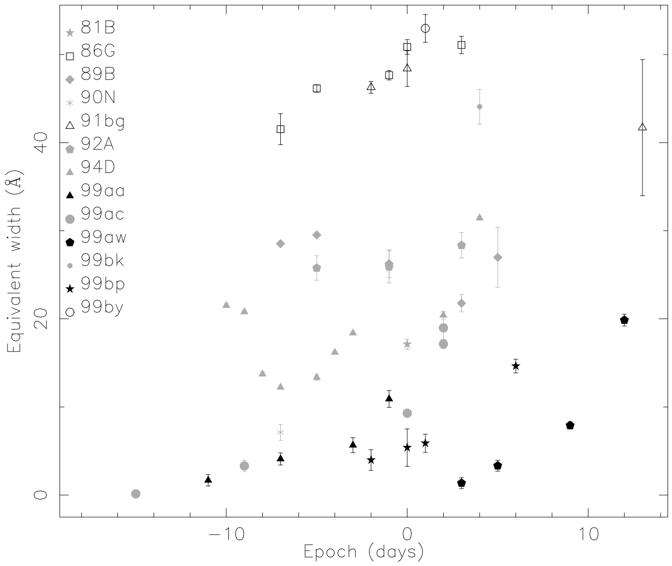

Fig. 10. Measured EW values corresponding to "Si II 5800". Error-bars are given by Eqn. 2 plus systematics arising in the continuum fit.

SNe Ia plus SN 1999ac, with greater Si II abundances and EW > 15Å. In average, there is a factor of 4 difference in EW between the two groups.

"Si II 5800" is very strong in under-luminous SNe, for which the main contribution might be due to the Na I D line (Filippenko et al., 1992). These SNe clearly separate

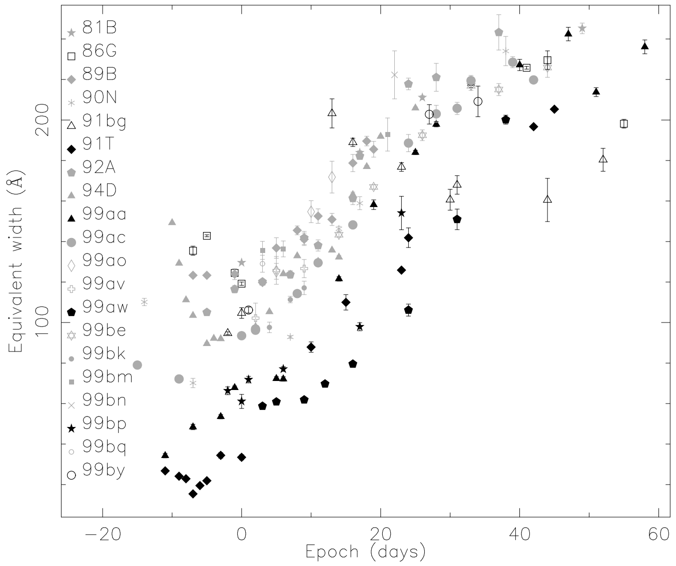

Fig. 11. Measured EW values corresponding to "Si II 6150". Error-bars are given by Eqn. 2 plus systematics arising in the continuum fit.

from the rest, with values of EW ≈ 50Å. The distinction between normal and 1991T/1999aa-like SNe is also found here, with a continuous change in EW between the two groups.

Less dispersion is found in the case of "Si II 6150". EW's scatter the most before maximum light, differing on a factor of 2 between extremes. Under-luminous SNe have absorption strengths similar to normal SNe up to 20 days past-maximum light. Afterward, they seem to stabilize (this is clearer in the case of SN 1991bg) while normal SNe keep increasing. 1991T/1999aa-like objects show significantly weaker "Si II 6150" before and around maximum light and become closer to normal SNe at later times (SN 1999aa becomes normal around two weeks after maximum, while SN 1991T and SN 1999aw do it later-on). SN 1999ac marks a division between 1991T/1999aa-like SNe and the rest along the whole evolution.

4.5. "Ca II H&K"

A peculiarity of the evolution of this feature is that the EW's do not increase in time for single SNe, as can be

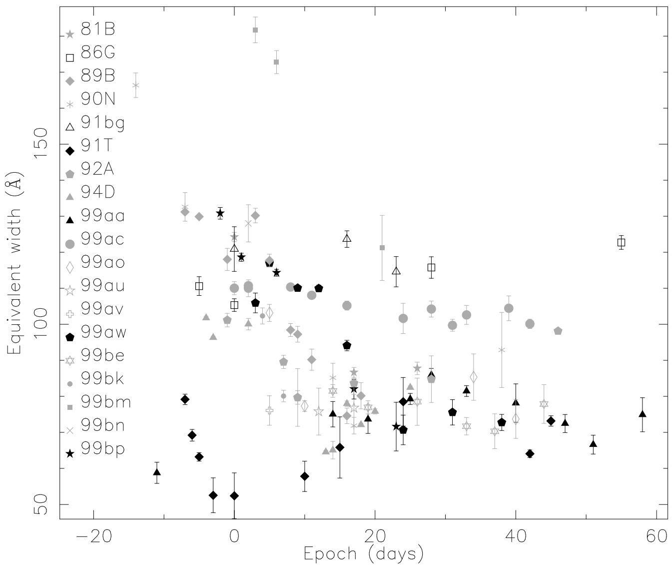

Fig. 12. Measured EW values corresponding to "Ca II H&K". Error-bars are given by Eqn. 2 plus systematics arising in the continuum fit.

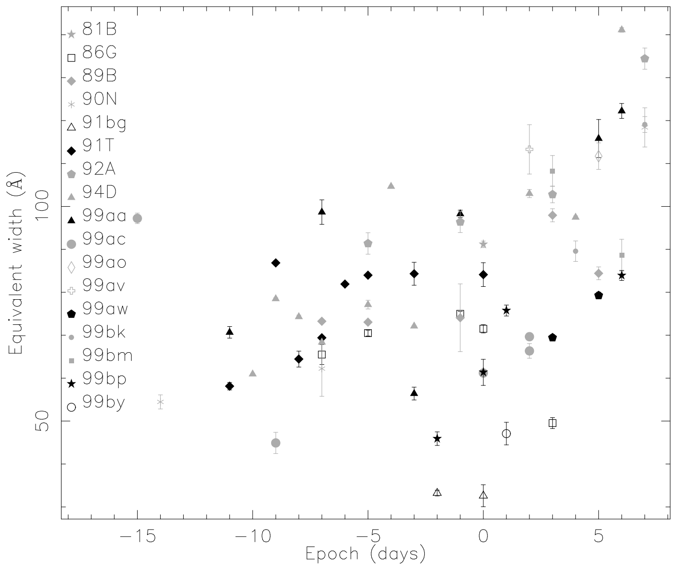

Fig. 13. Measured EW values corresponding to "S II W". Error-bars are given by Eqn. 2 plus systematics arising in the continuum fit.

seen in Fig. 12. The behavior is dependent on the object both qualitatively and quantitatively. The dispersion on EW is greater before maximum light, where some objects show an increase and other a decrease. After maximum light, there is normally a slow decrease, except for the under-luminous objects in which cases, EW's maintain or increase their values.

An additional peculiarity is that "Ca II H&K" breaks the usual trend relating absorption stregnths and lightcurve shapes seen in all of the previously analysed features. Here, before day 15, SN 1999aw and SN 1999bp show EW values similar to normal SNe while SN 1991T and SN 1999aa show very low values (SN 1991T has been suggested to lack Ca II at early stages, this feature having been identified as Ni II instead (Fisher et al., 1999)).

The case of SN 1999bm is worth noting. Its large EW values at early epochs are due to an unusually broad "Ca II H&K" feature. This phenomenon might be caused by the presence of a strong, high-velocity Ca II component, as in the case of the Ca II IR triplet for SN 2001el (Wang et al., 2003), although for SN 1999bm there is no evidence of such a component which should appear around 8000 Å.

4.6. "S II W"

The analysis of this feature is limited to the time range when it shows its distinct "W"-like shape, i.e. up to 7 days after maximum light. EW values are plotted in Fig. 13. Though the dispersion around maximum is large, the distinctions seen in previously discussed features are not present here. Under-luminous, normal and 1991T/1999aa-like SNe seem not to be distinguishable through this feature. This result may be an indication of the existence of a two-dimensional spectral classification of SNe Ia.

5. Conclusion

We have introduced EW measurements from SNe Ia spectra as an empirical tool to investigate the standard candle nature of these objects in a quantitative manner. We focused our analysis on three aspects: (a) Quantifying their spectral homogeneity. (b) Deriving empirical time evolution laws for their spectral features. (c) Searching for new secondary spectral calibrators of the standard candle. We defined eight spectral features and studied them separately.

Some features, namely "Fe II 4800","Mg II 4300" and "Ca II IR", show greater homogeneity than the rest. For those cases, homogeneity is quantified in terms of intrinsic dispersion around mean evolutionary curves. Time variations of the dispersion and thus of homogeneity among SNe are obtained for each of these three features. In the cases of "Fe II 4800" and "Ca II IR", dispersion around the mean curves reduce to less than 10% for epochs later than 15 days after B maximum. The behavior of individual objects is in general parallel to the mean curves. A general trend with increasing EW for increasing $\Delta m_{15}(B)$ is seen: SN 1999aw/1999bp – SN 1991T/1999aa – normal SNe Ia – under-luminous SNe Ia.

"Si II 4000", "Si II 5800" and "Si II 6150" show less uniformity while preserving the trend that correlates EW and lightcurve shapes. In these cases the distinction between normal and peculiar (both under-luminous and 1991T/1999aa-like) becomes clearer. "Si II 4000" shows the most evident distinction between 1991T/1999aa-like and normal objects. Under-luminous SNe are most clearly separated in "Si II 5800". "Si II 6150" is followed to later epochs and shows a dual behavior before and after Si II becomes contaminated by iron-peak lines around two weeks after maximum light. At early epochs it shows a larger dispersion, resembling "Si II 4000" and "Si II 5800". Later, 1991T/1999aa-like objects approach normal ones while under-luminous SNe stabilized. The case of SN 1999ac seems to divide under-luminous SNe from the rest.

The feature tagged as "Ca II H&K" differs from other features in two senses: (a) Its EW evolutionary behavior varies qualitatively among SNe and in general is not monotonically increasing. (b) The correlation between EW and $\Delta m_{15}(B)$ is not seen.

"S II W" shows large EW dispersion but no distinction according to lightcurve shape.

Through the analysis of "Fe II 4800", "Mg II 4300" and "Ca II IR" we define the spectroscopic parameters $\langle\Delta\mathrm{EW}\rangle_{\mathrm{Fe\ II\ 4800}}$, t_0 and $\langle\Delta\mathrm{EW}\rangle_{\mathrm{Ca\ II\ IR}}$, which correlate with the primary photometric parameter $\Delta m_{15}(B)$.

References

Branch, D. et al. 1983, ApJ, 270, 123

Cardelli, J. A., Clayton, G. C., & Mathis, J. S. 1989, ApJ, 345, 245

Filippenko, A. V. et al. 1992, AJ, 104, 1543

Filippenko, A. V. 1997, ARA&A, 35, 309

Fisher, A. et al. 1999, MNRAS, 304, 67

Folatelli, G. et al. 2003 in prep.

Gal-Yam, A. et al. 1999, IAU Circ. 7130

Garavini, G. et al. 2003 in prep.

Gómez, G., López, R., & Sánchez, F. 1996, AJ, 112, 2094

Gómez, G., & López, R. 1998, AJ, 115, 1096

Gray, D. F. 1992. *The observation and analysis of stellar photospheres*, Second Ed. Cambridge Univ. Press, 261

Hardin, D. et al. 2000, A&A, 362, 419

Hatano, K. et al. 2000, ApJ, 543, L49

Hillebrandt, W, & Niemeyer, J. C. 2000, ARA&A, 38, 191

Knop, R. et al. 2003 in prep.

Mazzali, P. A. et al. 1997, MNRAS, 284, 151

Nugent, P. et al. 1995, ApJ, 455, L147

Perlmutter, S. et al. 1999, ApJ, 517, 565.

Phillips, M. et al. 2002, astro-ph/0211100

Riess, A. et al. 1998, AJ, 116, 1009

Saha, A. et al. 2001, ApJ, 551, 973

Schaefer, B. E. et al. 1999, ApJ, 524, L103

Schlegel, D. J., Finkbeiner, D. P., & Davis, M. 1998, ApJ, 500, 525

Strolger, L.-G. et al. 2002, AJ, 124, 2905

Sullivan, M. et al. 2003, MNRAS, 340, 1057

Tonry, J. L. et al. 2003, astro-ph/0305008

Wang, L. et al. 2003, astro-ph/0303397